



HAL
open science

Analysis of Two Selected Solar Events in 2011 and 2015 With Mars Express Radio Occultation Data

Ananya Krishnan, Ozgur Karatekin, Sébastien Verkercke, Gregoire Henry,
Beatriz Sánchez-Cano, Olivier Witasse

► **To cite this version:**

Ananya Krishnan, Ozgur Karatekin, Sébastien Verkercke, Gregoire Henry, Beatriz Sánchez-Cano, et al.. Analysis of Two Selected Solar Events in 2011 and 2015 With Mars Express Radio Occultation Data. *Radio Science*, 2023, 58 (12), 10.1029/2023RS007784 . hal-04379497

HAL Id: hal-04379497

<https://hal.science/hal-04379497>

Submitted on 8 Jan 2024

HAL is a multi-disciplinary open access archive for the deposit and dissemination of scientific research documents, whether they are published or not. The documents may come from teaching and research institutions in France or abroad, or from public or private research centers.

L'archive ouverte pluridisciplinaire **HAL**, est destinée au dépôt et à la diffusion de documents scientifiques de niveau recherche, publiés ou non, émanant des établissements d'enseignement et de recherche français ou étrangers, des laboratoires publics ou privés.

Radio Science®

RESEARCH ARTICLE

10.1029/2023RS007784

Key Points:

- Effects of solar events on electron density are investigated using previously unexplored MaRS data with an in-house developed code
- The effects were observable on Mars's upper atmosphere for several weeks with a gradual decrease in M2 peak altitude for the 2011 event
- The overall trend of measured TEC variations was in accordance with the predictions, with no clear sign of variations due to solar events

Correspondence to:

A. Krishnan,
ananya.krishnan@student.uclouvain.be

Citation:

Krishnan, A., Karatekin, O., Verkercke, S., Henry, G., Sánchez-Cano, B., & Witasse, O. (2023). Analysis of two selected solar events in 2011 and 2015 with Mars Express radio occultation data. *Radio Science*, 58, e2023RS007784. <https://doi.org/10.1029/2023RS007784>


Received 22 JUN 2023

Accepted 26 NOV 2023

Author Contributions:

Conceptualization: Ozgur Karatekin
Funding acquisition: Olivier Witasse
Investigation: Ananya Krishnan
Methodology: Ozgur Karatekin
Software: Ananya Krishnan, Sebastien Verkercke, Gregoire Henry, Beatriz Sánchez-Cano
Supervision: Ozgur Karatekin, Olivier Witasse
Validation: Ananya Krishnan, Sebastien Verkercke, Gregoire Henry
Writing – original draft: Ananya Krishnan
Writing – review & editing: Ozgur Karatekin, Beatriz Sánchez-Cano, Olivier Witasse

Analysis of Two Selected Solar Events in 2011 and 2015 With Mars Express Radio Occultation Data

Ananya Krishnan^{1,2} , Ozgur Karatekin¹, Sebastien Verkercke³, Gregoire Henry¹, Beatriz Sánchez-Cano⁴, and Olivier Witasse⁵

¹Royal Observatory of Belgium, Uccle, Belgium, ²Earth and Life Institute, UCLouvain, Louvain-la-Neuve, Belgium,

³Laboratoire atmosphères, Milieux, Observations spatiales, LATMOS, Paris, France, ⁴School of Physics and Astronomy, University of Leicester, Leicester, UK, ⁵European Space Agency, ESTEC, Noordwijk, The Netherlands

Abstract The temporal behavior of the Martian ionosphere is highly variable due to various dynamic processes including space weather events. Here, we study the effect of solar flares and coronal mass ejections (CMEs) on the Martian ionosphere for two selected solar events in 2011 and 2015, using the publicly available Mars EXpress (MEX) radio occultation (RO) data (MaRS). We developed a data processing software that converts the calibrated Radio Occultation (RO) Doppler data to scientifically valuable atmospheric profiles. Using this software and previously unexplored MaRS observations, the variations in ionospheric parameters (electron density profiles and total electron content (TEC)) are calculated in order to evaluate the ionospheric changes due to solar flares and CMEs. The RO measurements mostly available 1–4 days apart from the peak events, showed no evident change in the TEC nor in the shape of electron density profiles except for a possible gradual decrease in altitude of M2 (main layer) peak density following the arrival of CMEs. To better quantify the effect of solar events on electron density profiles, RO observations near the time of arrival of solar flares and CMEs are crucial. This can be achieved by frequent RO measurements by various Mars orbiters including spacecraft-to-spacecraft measurements assisted by multi-instrument monitoring of the ionosphere.

1. Introduction

Space weather events are a major source of energetics, short-term dynamics, and the evolution of planetary atmospheres. Solar Energetic Particles (SEPs) are high energy electrons, protons and heavy ions originating from Sun. SEPs penetrates Earth's magnetic field causing enhanced ionization in the ionosphere and occasionally modifies the chemistry of the polar atmosphere (Klein & Dalla, 2017). The two major kinds of eruptions on Sun are the solar flare and Coronal Mass Ejections (CMEs). Both affect planetary atmospheres. Solar flares are defined as abrupt and intense eruptions of electromagnetic radiation in Sun's atmosphere, the result of which is emission across a broad spectrum. A CME, often associated with a solar flare, is a large ejection of plasma and magnetic field from Sun's corona to the interplanetary space. When CMEs propagate through the interplanetary medium, or solar wind, they are referred to as interplanetary coronal mass ejections (ICMEs). Fast ICMEs have upstream shocks which accelerate ions to 10 keV to 10 MeV. The energy and X-rays produced by the solar flare can reach Earth and Mars at the speed of light in the order of 10 min whereas the coronal mass ejections carrying cloud of solar material takes usually several days (Kawabata et al., 2018; Morgan et al., 2014; Tsurutani et al., 2009).

A planet's interaction with the Sun is a function of the heliocentric distance, chemical composition, and intrinsic magnetic field of the planet. Many different studies have been conducted to understand the effect of solar events on Earth's ionosphere. Such studies have shown that enhanced flux of solar particles during a solar flare causes increased ionization in Earth's ionosphere (Tsurutani et al., 2009). ICME results in shock compression of the Earth's magnetosphere, energizing magnetospheric electrons and ions. Thus leading to an increase in energetic particle precipitation into the ionosphere causing a sudden increase in electron density and formation of auroras (S. A. Haider et al., 2009). Similarly, S. Haider (2012), reports during the solar flare that occurred on 13 May 2005, they observed that the lower ionosphere (~112 km) showed an increase in total electron content (TEC) and the CME associated with the flare compressed the magnetosheath of Mars by about 15 km. However, unlike Earth, Mars has little or no intrinsic magnetic field. The only sources of magnetic field on Mars are the strong pockets of crustal magnetism (Lillis et al., 2008) and the highly dynamic, induced magnetic field created by the interaction between the magnetized solar wind and the ionosphere (Riedler et al., 1989). Therefore, the solar wind directly interacts with the ionosphere. Thus space weather dependence of the martian ionosphere becomes a key

and fundamental issue in ionospheric physics, providing information essential to understand the variations in the ionosphere and its processes.

The ionosphere of Mars owes its existence to the photoionization of neutral species by solar extreme ultraviolet (EUV) and soft X-ray photons (Fox et al., 2008; Nagy & Banks, 1970). It has a stratified structure with two main layers in its electron density profile (N_e). The primary layer (M2 layer) is formed by solar EUV radiation ($\approx 20\text{--}90$ nm) and has a peak electron density at around 120–140 km altitude with a peak density of $\approx 10^{11}\text{m}^{-3}$ at the sub-solar point. The second layer (M1 layer) occurs at a lower altitude with a peak electron density of $\approx 10^9\text{m}^{-3}$ and is formed by solar soft X-ray and electron impact ionization. The peak electron density magnitude and altitude are highly variable. Dust storms, solar cycles, solar flares, and coronal mass ejections (CMEs) are the major sources of ionospheric variabilities. The analysis of such variations will help us understand atmospheric loss by solar wind stripping, which has had great impacts throughout the history of Mars (Witasse et al., 2008).

Radio occultation (RO) is the sole technique available for global profiling of vertical electron densities from satellite orbit heights down to the bottom of the ionosphere (Jakowski, 2005). Its vertical range and resolution (typically ≈ 500 m for MEX) are exceptional (Pätzold et al., 2004). RO experiments precisely measure the Doppler shift observed on the link between a planetary spacecraft and Earth, as the spacecraft passes into occultation behind the planet. This measured data can be processed to extract the vertical electron density profiles of the ionosphere (Eshleman, 1973; Fjeldbo et al., 1970; Kliore et al., 1965) and is largely used to investigate the variabilities in electron density profiles.

RO measurements for the study of the Martian ionosphere were first performed by Mariner 4 in 1965 (Kliore et al., 1965). Since then RO experiments have been an integral part of most of the Mars missions. Pätzold et al. (2004), Withers et al. (2014), Zhang et al. (2015), Pätzold et al. (2016), Wang et al. (2018), and Kerstin et al. (2021) have independently retrieved electron density profiles using RO data. They all use the well-established approach to obtain the electron density profiles, that is to first retrieve the refractivity profile of the ionosphere from the bending angle of the radio wave through Abel integral inversion assuming an axisymmetric atmosphere. Here, we also use the same method assuming a spherically symmetrical atmosphere. The details of the method are given in Section 2.

The RO measurements on Mars have been studied to investigate the variations of electron density with the above-mentioned sources of variabilities. Felici et al. (2020) showed the behavior of the Martian ionosphere using ROSE (Radio Occultation Science Experiment) on Mars Atmosphere and Volatile Evolution (MAVEN) in the event of dust storms. Several previous studies have also reported the enhancement and reduction of the Martian ionosphere during solar events (Jakosky et al., 2015; Lee et al., 2017; Thampi et al., 2021). Investigating the effect of solar energetic particle (SEP) events on the Martian ionosphere using Mars Global Surveyor (MGS) electron reflectometer and RO, Ulusen et al. (2012) observed no obvious/clear effect on the upper ionosphere, but a small increase in electron density below 100 km altitude for some events. However, conclusive evidence to relate these effects to a SEP event is missing. Contrary to this, Mendillo et al. (2006), noticed a strong enhancement in the ionosphere with relatively more pronounced enhancement at lower altitudes during a solar flare event. Nevertheless, a complete comprehension of the Martian ionospheric response to a solar event is still lacking. This is vital in understanding the temporal evolution of the planetary atmosphere (Withers et al., 2022).

Here, we study the impact of solar energetic particles (SEPs) on Mars atmosphere at two distinct event observed on June 2011 and mid-February–March 2015. The 2011 event was associated with a single flare and ICME (Morgan et al., 2014) while the 2015 event includes a series of ICMEs and flares (Jakosky et al., 2015). Using our own RO data analysis software, developed at the Royal Observatory of Belgium (ROB) (hereafter, “ROB” refers to the results or output obtained using this software), we analyze the publicly available Mars EXpress Radio Science (MaRS) data from ESA’s Planetary Science Archive (PSA) (see Section 2). For both events, the temporal variations of total electron content (TEC) and electron density profiles are retrieved from these previously unexplored MaRS observations to quantify the ionospheric response due to solar flares and CMEs.

2. Analysis Method and Data Set

2.1. Two-Way Radio Occultation

Radio occultation experiments on Mars have been performed in one-way mode or two-way mode depending on the precision of the onboard clock (Withers et al., 2014; Withers & Moore, 2020). In this study, we use the two-way mode experiments conducted by MaRS. The analysis method of the two-way RO experiment is very similar to the classical one-way method (Pätzold et al., 2004, 2016; Withers et al., 2020). In a two-way RO experiment, the ground station at Earth sends a coherent uplink radio frequency, which is received and re-transmitted

back to Earth after multiplying it with a constant transponder ratio (turn-around ratio). Thus, the signal passes through the planetary atmosphere twice. The received frequency is recorded and stored as a function of ground received time. As the received signal is derived from the uplink signal with a known frequency shift, the changes in radio path length can be measured by comparing the received signal with the original uplink signal. This measured Doppler shift in the radio link is used to find the refractivity of the atmosphere.

In our analysis, a spherically symmetrical atmosphere is assumed, similar to the previous Mars studies of Fjeldbo et al. (1971), Pätzold et al. (2004), Wang et al. (2018), and Withers et al. (2020). In a spherically symmetric atmosphere with refractivity of the medium varying as a function of height, the radio wave propagating through it bends about the center of the system. Following the same methods of previous studies, the vertical electron density profiles are retrieved from RO measurements using Abel transformation. The residual Doppler frequency we use is the level 2 data, which is already corrected for the propagation of the signal in space and Earth's atmosphere. One of the major steps while processing this calibrated RO data is the baseline correction applied to the frequency residual (Wang et al., 2018; Withers et al., 2020). The baseline correction is performed in two parts. The first step is to identify the threshold altitude, that is the altitude above which the ionosphere is absent and, to set the frequency residual above this altitude to be zero. The second baseline correction is performed after obtaining an initial refractivity profile. The second baseline correction is carried out to make sure that the transition region between the ionosphere and neutral atmosphere has zero electron density (see Withers et al. (2020)).

The net Doppler shift received at the ground station from Mars ionosphere can be expressed as

$$df_{i,jj} = df_{i,jup} \cdot k_j + df_{i,jdn} \quad (1)$$

where df is the Doppler shift, the indices i denotes the ionosphere, and j denotes the frequency band (X or S). For example, “XX” would correspond to both uplink and downlink signals in X-band, whereas “ j_{up} ” and “ j_{dn} ” would refer to the uplink and downlink segments of the radio link, respectively. The factor k_j is the frequency multiplier that the spacecraft applies to convert the uplink signal to the downlink signal. It is given as $k_X = 880/749$ and $k_S = 240/749$.

The Doppler shift from the ionosphere depends inversely on the signal frequency, therefore

$$df_{i,jup} = df_{i,jdn} \cdot k_j \quad (2)$$

Combining the above two equations, we have

$$df_{i,jdn} = \frac{df_{i,jj}}{(1 + k_j \cdot k_j)} \quad (3)$$

One can determine $df_{i,jj}$ from the recorded data by taking the difference between the frequency of the downlink signal received on the ground and the predicted frequency that would have been observed if Mars had no ionosphere. So, then by using Equation 3, we have the one-way Doppler shift caused by the ionosphere at the received downlink frequency.

It is also possible to obtain the downlink Doppler shift using differential Doppler shift (ddf) if the spacecraft can transmit two different radio frequencies (e.g., X and S-band) like MEX (Pätzold et al., 2016), then

$$ddf = df_{i,XS} - \frac{3}{11} \cdot df_{i,XX} \quad (4)$$

where $11/3$ is the constant transponder ratio of $880/240$. The advantage of using differential Doppler is that it removes all non-dispersive noise sources.

In our analysis, we used both the X and S band signals as well as the differential Doppler. Figure 1 shows that all three frequency bands give the same electron density profile. In the Results Section, we present only the X-band signals which are much less noisy.

2.2. Comparison With Previous Studies

The electron density profiles retrieved with the analysis method explained above are compared with the previously published results by the MEX—MaRS team as well as the MAVEN - ROSE team. Both MaRS and ROSE conduct RO experiments with spacecraft components consisting of a radio transceiver and a High Gain Antenna (HGA). At the ground, the radio signals are transmitted and received using ESA's Estrack and/or NASA's Deep Space Network

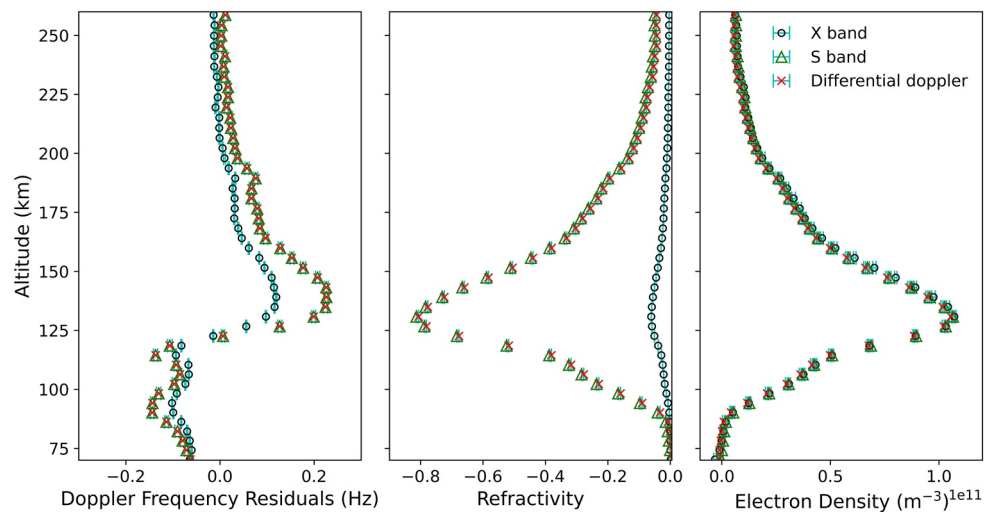


Figure 1. The raw Doppler residual frequency (first panel), the refractivity (second panel), and the electron density (third panel) with X-band, S-band, and differential Doppler frequencies for the data set MEX-MRS-1-2-3-EXT1-0895-V1.0 (25/03/2006). The effect of the ionosphere on a radio wave propagating through it is inversely proportional to the carrier frequency (X/S—band) and the differential doppler scenario behaves similarly to the S-band. However, in the end, we obtain the same electron density for all three cases as the electron density is calculated by dividing the refractivity with the carrier frequency. Please note that the measurement uncertainties indicated by light blue lines are small compared to the marker symbols and might not be apparent in the graph.

(DSN) radio antennas (34 and 70 m). MaRS uses simultaneous and coherent dual-frequency downlinks at X-band and S-band, whereas, MAVEN - ROSE uses a single frequency (X-band) to conduct RO experiments. Both MEX and MAVEN use an elliptical orbit. MAVEN - ROSE makes observations in both ingress (spacecraft disappearing behind the planet as seen from Earth) and in egress (spacecraft re-appearing from behind the planet as seen from Earth) with occultation opportunities occurring once per orbital period of approximately 4.5 hr (Withers et al., 2020). Whereas, MaRS primarily makes ingress observations with 1–2 occultations per sol (1 sol = 1.028 Earth days).

The left panel of Figure 2 shows a comparison of ROB electron density with two published MaRS profiles available in the Planetary Data System (PDS) <https://pds-geosciences.wustl.edu/mex/mex-m-mrs-5-occ-v1/>. Whereas, Figures 2e and 2f, correspond to ROSE profiles obtained for an ingress occultation, and Figures 2g and 2h show the ROSE profiles for an egress occultation. The details of the data sets are given in Table 1. The complete set of ROB electron density profiles for the MaRS observations are provided at <https://doi.org/10.17605/OSF.IO/MXHCG> along with the ROB output data files investigated for 2011 and 2015 solar event data. The results obtained with average bending angle and impact parameters for uplink and downlink signals show very good agreement with the MaRS data (see Figures 2a–2d) as was the case for Wang et al. (2018). The differences between the profiles are two orders of magnitude less than the actual electron density measurements. These small differences may be attributed to user-dependent parameters like the threshold altitude for the baseline correction, the upper limit of integration used to calculate the refractivity or the numerical model used for Abel integration.

Withers et al. (2020) gives a detailed explanation with threshold altitude and fit parameters for selected ROSE profiles. Following the same approach, we obtained an excellent match with the electron density profiles published in Withers et al. (2020), Figures 2e–2h.

2.3. MaRS Data Set for Selected Solar Events

We identified two well-reported major solar events during which several MaRS measurements were made. The first event happened in June 2011 (Morgan et al., 2014) over a period of 1 week and the second started in mid-February 2015 (Jakosky et al., 2015; Lee et al., 2017) with perturbations lasting for over two weeks.

The MaRS data used in this study are presented in Table 2. The previously unexplored data set includes five MaRS measurements for 2011 and 11 for 2015. The RO measurements have similar solar zenith angles (SZAs) and local solar times (LSTs), that is 72° and 7.2 hr, for 2011, and, 83° and 19 hr for the 2015 event. The locations of these MaRS measurements are shown in Figure 3 with the remnant crustal magnetic field on the background.

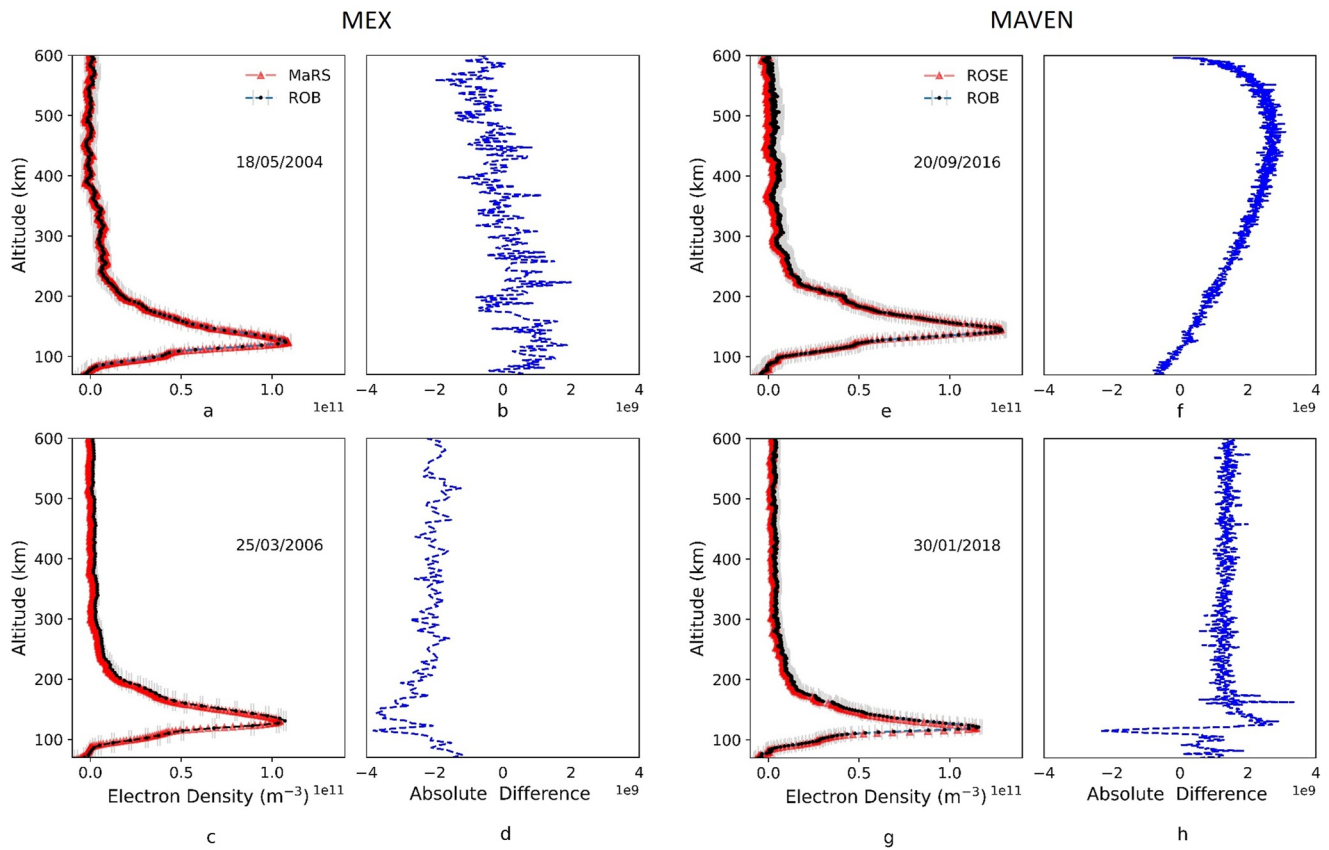


Figure 2. (a) Comparison and (b) absolute difference of ROB (in blue) and MaRS published electron density (Pätzold et al., 2004) (in red) for 18 May 2004, similarly (c) comparison and (d) absolute difference for 25 March 2006. (e) Comparison and (f) absolute difference of ROB results with published results of MAVEN ROSE (Withers et al., 2020), an example for ingress occultation (20 September 2016), (g) and (h) same analysis for an egress observation (30 January 2018). Red dots represent 13 level (electron density profiles) data from ROSE and the black dots correspond to ROB output.

The MaRS L2 level (residual Doppler) measurements are obtained from PSA which contain more than 1,000 profiles collected over a long period (>15 terrestrial years). We processed the selected observations (Table 2) to high-level products (i.e., refractivity, pressure, temperature, electron density) using the method described in Section 2.1. The results are presented in the next Section.

3. Results

3.1. MaRS Electron Density Profiles for June 2011 Event

The 2011 June solar event occurred when the Sun unleashed an M2 solar flare, a minor radiation storm (also known as a solar energetic particle (SEP) event), and a CME. Perturbations in Mars' ionosphere as a response to

| Date | Data ID | Latitude | Longitude | SZ (°) | LST (hrs) | L_s (°) |
|------------|-----------------|----------|-----------|--------|-----------|-----------|
| | | (°N) | (°E) | | | |
| 18/05/2004 | MEXMRS_046 | 53.6 | 272.6 | 70.2 | 17.0 | 35.1 |
| 25/03/2006 | MEXMRS_0895 | 20.5 | 216.3 | 54.0 | 15.7 | 30.2 |
| 20/09/2016 | MVNRSE_20160920 | -70.4 | 45.8 | 58.8 | 14.9 | 226.6 |
| 30/01/2018 | MVNRSE_20180130 | 18.0 | 33.2 | 55.5 | 8.0 | 122.6 |

Table 2
Date, Data ID, Latitude, Longitude, SZA, LST, and L_s of 2011 and 2015 Data Sets Used in This Paper

| Date | Data ID | Latitude | Longitude | SZA | LST | L_s |
|------------|-------------|----------|-----------|------|-------|-------|
| | | (°N) | (°E) | (°) | (hrs) | (°) |
| 11/06/2011 | MEXMRS_2936 | 0.3 | 294.9 | 72.8 | 7.2 | 308.9 |
| 11/06/2011 | MEXMRS_2938 | -1.6 | 192.7 | 72.5 | 7.2 | 309.1 |
| 12/06/2011 | MEXMRS_2939 | -4.7 | 348.3 | 72.2 | 7.2 | 309.4 |
| 12/06/2011 | MEXMRS_2941 | -6.9 | 246.0 | 71.8 | 7.1 | 309.6 |
| 14/06/2011 | MEXMRS_2946 | -14.9 | 352.8 | 71.0 | 7.0 | 310.6 |
| 16/02/2015 | MEXMRS_3696 | -61.7 | 148.5 | 87.3 | 20.9 | 292.2 |
| 19/02/2015 | MEXMRS_3697 | -59.9 | 98.7 | 86.4 | 20.4 | 294.2 |
| 23/02/2015 | MEXMRS_3700 | -57.6 | 204.9 | 85.4 | 19.9 | 296.5 |
| 26/02/2015 | MEXMRS_3701 | -55.3 | 156.9 | 84.6 | 19.6 | 298.4 |
| 02/03/2015 | MEXMRS_3703 | -52.4 | 265.1 | 83.9 | 19.3 | 300.7 |
| 05/03/2015 | MEXMRS_3706 | -49.9 | 218.8 | 83.3 | 19.0 | 302.6 |
| 12/03/2015 | MEXMRS_3710 | -44.1 | 282.9 | 82.3 | 18.6 | 306.7 |
| 16/03/2015 | MEXMRS_3712 | -41.0 | 33.4 | 81.9 | 18.4 | 308.9 |
| 19/03/2015 | MEXMRS_3713 | -38.3 | 348.6 | 81.7 | 18.3 | 310.8 |
| 26/03/2015 | MEXMRS_3714 | -32.5 | 55.4 | 81.3 | 18.0 | 314.9 |
| 30/03/2015 | MEXMRS_3716 | -29.3 | 166.7 | 81.2 | 17.9 | 317.0 |

these events were detected by instruments of MEX and Mars Odyssey (Morgan et al., 2014). The Mars Advanced Radar for Subsurface and Ionosphere Sounding (MARSIS) (Gurnett et al., 2005) on board the MEX spacecraft measured the local densities and magnetic field strengths, indicating an enhancement of 100-eV electrons. Local density and magnetosheath electron measurements and remote soundings show compression of ionospheric plasma to lower altitudes due to increased solar wind dynamic pressure associated to the CME. MARSIS topside sounding of the ionosphere indicates that it is extended well beyond the terminator, to about 116° solar zenith angle, in a highly disturbed state. This extension may be due to an increased ionization owing to SEPs and

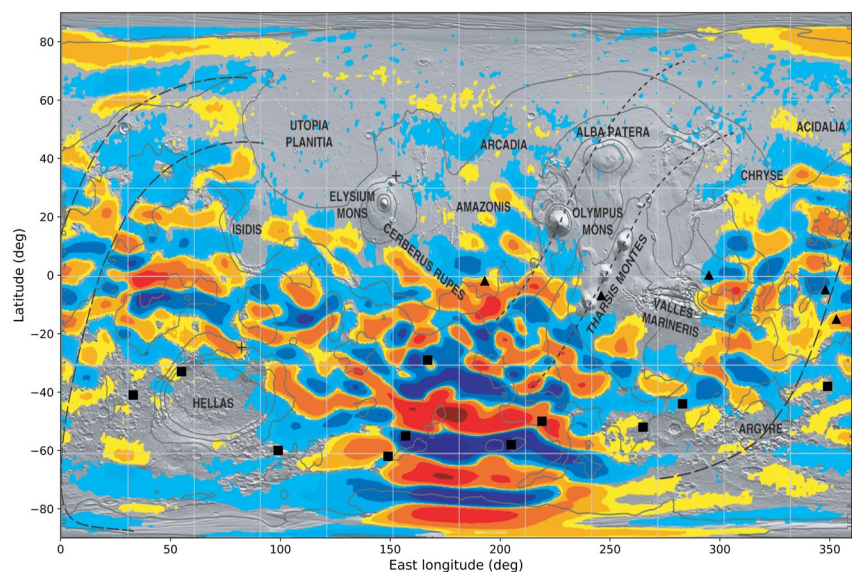


Figure 3. The location of all the MaRS data used in this paper are represented by black triangles (for the 2011 event) and black squares (for the 2015 event). The background map (Connerney et al., 2005) represents the crustal magnetic field of Mars observed by the Mars Global Surveyor satellite.

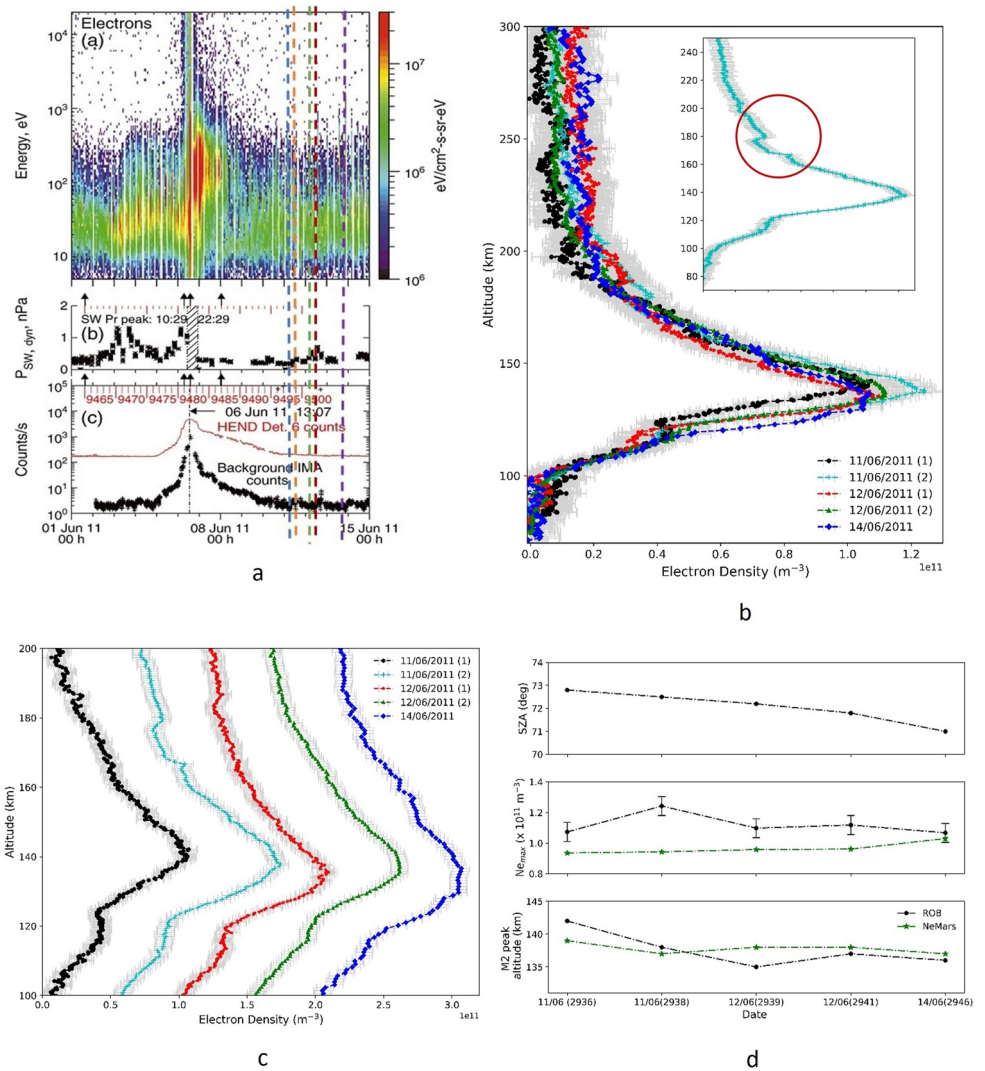


Figure 4. (a) Shows the timeline of data set with respect to the peak activity of solar event that occurred on 6 June 2011 (Morgan et al., 2014), (b) electron density profiles calculated in the present study from MEX–RO, inset: zoomed electron density profile for the second measurement on 11 June 2011, showing the change in slope (c) the electron density profiles in (b) shifted with 0.5 units along the x-axis for better interpretation, and (d) variation of SZA, M2 peak density, and M2 peak altitude for the five MaRS profiles, calculated in the present study compared with the NeMars model. The NeMars give these parameters without taking the solar event into consideration. More details of NeMars are explained in Section 3.3.

magnetosheath electrons or to plasma transport across the terminator. The surface reflection from both ionospheric sounding and subsurface modes of the MARSIS radar was attenuated, indicating increased electron content in the Mars ionosphere at low altitudes, where the atmosphere is dense. Morgan et al. (2014) makes a very detailed analysis of these observations.

Figure 4a, shows the electron energy-time spectrogram, solar wind dynamic pressure, and background counts from the Analyzer of Space Plasma and Energetic Atoms (ASPERA -3) (Barabash et al., 2006) onboard MEX, as well as charge particles count from High Energy Neutron Detector (HEND) (Hurley et al., 2008) on board Mars Odyssey. This indicates that the event began on 5 June, peaking on the 6th and then trailing off around 15 June 2011. MaRS has five observations in this period, with two observations several hours apart on 11, and 12 each, and one observation on 14 as marked with colored vertical lines in Figure 4a. They occur not at the peak moment, but when the ionosphere has mostly recovered from the space weather event. Therefore, here, we expect to see the last stage of the recovery.

The electron density profiles of all the five MaRS observations are shown in Figure 4b in linear scale. Withers et al. (2012) reports variations in the vertical extent of the ionosphere at the occurrence of CMEs and the high

flux of SEPs at Mars, however, we see no such abrupt change in the overall structure and shape of the profiles. The comparison between the profiles shows M2 peak density is very consistent with M2 peak electron density in the range 1.12×10^{11} el. $\text{cm}^{-3} \pm 10\%$ (Figure 4d (middle panel)). Also, the lower part of the profiles remains unchanged. However, the altitude at which the M2 peak occurs decreases over time, see Figure 4c. There is a decrease of about 6 km, with the first observation having the M2 peak at an altitude of 142 km and the last observation on the 14 June having the peak at 136 km (Figure 4d (bottom panel)). In addition, Figure 4d, also show NeMars model (see Section 3.3) calculated M2 peak density and altitude in the absence of any solar event as green points for comparison. It is evident from Figure 4a that the SEP perturbation almost completely decayed on 14 June 2011. The observed decrease in peak altitude can be associated with the relapse of the ionosphere back to its normal state after the solar event.

The slope of the density profiles is unaffected except for the second profile on 11 June. For this particular measurement, we see an abrupt change in slope at around 175 km as shown in the inset of Figure 4b. However, we have to take into account that this measurement is made over a region of strong crustal magnetic field. Gurnett et al. (2008) reports that the vertical magnetic fields in such regions connect with the solar wind and thereby heat up the lower levels of the ionosphere. This in turn results in increased scale height and electron density. Therefore, we cannot completely suppose that the change in scale height and slightly higher electron density observed for this measurement is an effect of the solar event.

3.2. MaRS Electron Density Profiles February–March 2015 Event

The CME that impacted Mars in February–March 2015 is one of the strongest observed solar events. Jakosky et al. (2015) and Lee et al. (2017) reports that several MAVEN instruments observed this event. A series of solar flares, an influx of SEP ions, SEP electrons, and CME occurred during a period starting from mid-February to the end of March 2015. Figure 5a gives an overview of the series of events impacting Mars during the time period from 1 February to 13 March 2015. Figure 5b shows the major space weather events impacting Mars during the period from 16 February to 30 March 2015.

The series of events began on 9 February 2015, with an M2 class flare detected by MAVEN EUV monitor (EUVM) (Eparvier et al., 2015). On 11 February 2015, SEP ions with ~ 100 keV to ~ 1 MeV and SEP electrons of energies < 100 keV were detected by MAVEN (Lee et al., 2017). From 18 to 23 February, short periods of SEP activities were also observed. Later on 24 February, a CME erupted on Sun, with its shock arrival observed on Mars on 27 February. This was observed by MAVEN as a major solar wind density enhancement with a peak solar wind density of ≈ 23 cm^{-3} , dynamic pressure of ≈ 4.5 nPa and total Interplanetary Magnetic Field (IMF) of ≈ 11 nT (Lee et al., 2017). Two M-class flares and one of the largest X-class flare events were observed by MAVEN on 28 February and 1 March respectively. An influx of SEP electrons and ions was detected on 2 and 3 March with energies measured at < 100 keV electrons and 1 MeV. MAVEN again observed two CME arrivals on 4 and 7 March. Furthermore, the EUVM observed an M2-class flare peaking on 6 March 2015. Figure 5a shows that SEPs accelerated by the new activity reached Mars. Thereafter, for several days the condition at Mars seems to be pretty quiet until an M3.0 flare event was observed on 24 March 2015 by EUVM (Lee et al., 2017). A thorough explanation of the observations made by different MAVEN instruments in detecting each event in this series could be found in Lee et al. (2017) and Jakosky et al. (2015).

MaRS has 11 observations in this 7 weeks period. The electron density profiles are divided into three time periods (16–26 February, 2 to 12 March, and 16 to 30 March) in Figures 5c–5e only for the sake of clarity. From Figures 5c–5e, we see that the overall shape of the electron density profile did not change in any of the observations. Looking at the timeline of the event (Figures 5a and 5b), we can infer that 16 and 19 February as well as 16, 19, and 30 March 2015 are comparatively quiet days with less solar activity. Furthermore, 23, 26 February, and 5, 30 March measurements were taken over regions of strong crustal magnetic fields.

The profiles shown in Figure 5c correspond to relatively quiet periods and we observe similar electron density profiles.

The middle panel, Figure 5d exhibits MaRS profiles during the most active period of this series. All three profiles in this panel show similar M1 and M2 peak densities and peak altitudes, but different topside ionosphere. The slope of the graph, above approximately 200 km, changes for the 5 and 12 March profiles before they join back the March 2 profile around 300 km.

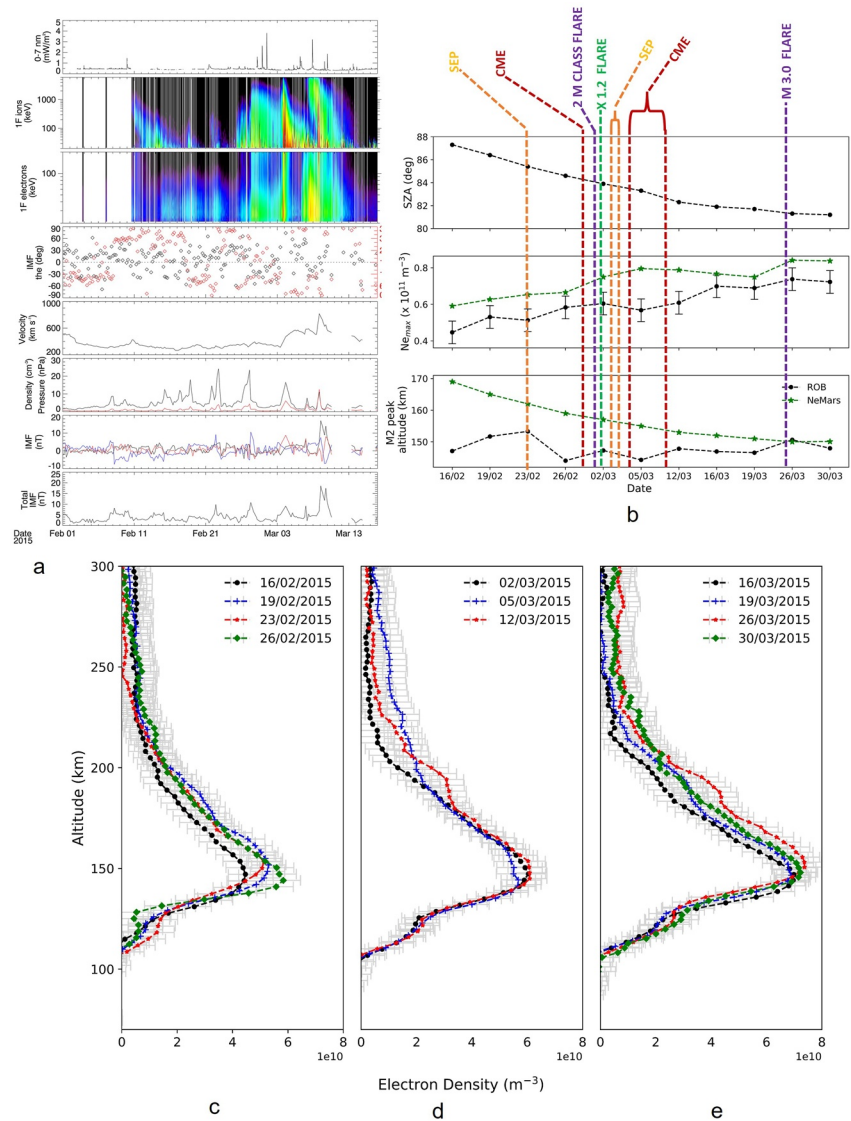


Figure 5. (a) The EUVM solar 0.1–7 nm irradiance data, differential energy fluxes for the SEP ions and electrons, solar wind velocity, density and dynamic pressure from SWIA and interplanetary magnetic field from MAG for the period 01 February to 13 March 2015 (Lee et al., 2017), (b) The SZA, M2 peak density, and M2 peak altitude obtained in the present study from MEX-RO data (shown in black circles) with solar events (vertical dashed lines). The M2 peak density and M2 peak altitude are compared with the NeMars model (green). The NeMars give these parameters without taking the solar event into consideration. More details of NeMars are explained in Section 3.3. The electron density profiles obtained from MaRS data in linear scale for the period (c) 16 to 26 February, (d) 2 to 12 March, and (e) 16–30 March 2015.

Lastly, in Figure 5e, the M2 and M1 peak densities are similar for all the data. The 26 and 19 March profiles show a very similar jump in the graph around 200 km, as observed in the 12 March profile. Relatively, for the 26 March profile, an increase in M2 electron density is observed. The M1 layer is produced by the absorption of soft X-ray photons. A single photoelectron produced by a soft X-ray photon produces multiple ion-electron pairs as it thermalizes in collisions with neutral species. Hence electron impact ionization is a critical process in the M1 layer, but is less critical in the M2 layer, although not negligible (Withers et al., 2023). The slight increase in M2 electron density for 26 March 2015 observed here was preceded by a M class flare. We also notice that all the available MaRS data for the March 2015 solar event are 1–4 days earlier or later than the peak of the event.

Figure 5b, gives an overview of the variation of SZA (top panel), M2 peak density (middle panel) and M2 peak altitude (bottom panel) for the 11 observations along with the time line of the major events. The green points in middle and bottom panels of Figure 5b, represents the NeMars model (see Section 3.3) calculated parameters in the absence

of any solar event. It shows that the RO calculated M2 peak density follows a very similar trend as that of the model calculated peak density. The RO calculated M2 peak altitude varies in the range 148 ± 5 kms. Here, the principal variation of M2 peak density and M2 peak altitude is correlated with SZA. The flare may increase the M2 peak altitude whereas the effect of CME and other SEP are less obvious. The effects of solar events on electron density are difficult to observe due to the scarce data points and the relatively large time delay of observation following the event.

3.3. TEC Variation During Solar Events

The existing empirical model of Mars upper atmosphere helps to predict how the ionosphere would behave in the absence of any solar event. In this Section, we compare the ionospheric total electron content (TEC) deduced from RO data by integrating the electron densities with two empirical TEC models—NeMars (Sánchez-Cano et al., 2013) and MoMo (Bergeot et al., 2019). NeMars is an empirical model based on the Active Ionospheric Sounding mode (AIS) of MARSIS and Mars Global Surveyor (MGS) RO data. It predicts the main characteristics of the photo-chemical region (the two main layers) of the ionosphere according to Chapman's formulation. It provides the electron density profile, the peak altitude, peak density, scale height (increase in altitude for which the density and pressure decrease by a factor of e), and TEC (Sánchez-Cano et al., 2013). MoMo based on the subsurface mode of MARSIS radar, provides the vertical TEC for a specified location, time, and solar activity level (Bergeot et al., 2019). Both models use $F_{10.7}$, solar flux as a proxy to solar activity, however, they do not take into account any effect of SEPs, solar flares, CMEs, or the crustal magnetic field.

According to Chapman's formulation, the photo-chemically controlled region of the ionosphere can be represented with a constant scale height (H). However, H itself varies with altitude and therefore, NeMars uses a scale height that varies linearly with altitude. NeMars have options to keep the scale height constant or vary it linearly depending on the solar cycle phases (Sánchez-Cano et al., 2016). However, for all the analyses presented in this paper, we have used the model with a scale height that varies constantly with altitude (Sánchez-Cano et al., 2013).

The predicted TEC by the NeMars and MoMo is compared with the MaRS analysis of the present study in Figure 6. All the TEC values mentioned in this paper are normalized using the highest TEC value as a benchmark.

For a time period without any solar events or crustal magnetic fields, the predictions and observations show good overall agreement (Figure 6a). The empirical models slightly overestimate the TEC. The average difference between ROB TEC and NeMars TEC is 0.11 and it is 0.04 for MoMo TEC. The data points shown in Figure 6 as blue diamonds represent the data collected over locations with the crustal magnetic field. Previous studies have shown that observed TEC is higher in strongly magnetized regions (Dubinin et al., 2016). However, we do not see an enhancement of TEC above the crustal field regions either in the observations or in the models.

Figures 6b and 6c compare the normalized TEC from RO observations with the TEC from the empirical models, in the presence of solar events. During the 2011 event, no clear effect of the solar event is distinguishable on RO observations (Figure 6b). The mean difference between ROB TEC and NeMars TEC is 0.07 and it is 0.03 for MoMo TEC. The difference between models and observation is larger during the 2015 event with mean differences of 0.16 and 0.19 for TEC—NeMars TEC, and ROB TEC—MoMo TEC respectively. In particular around 23, 26 February, and 16, 19 March the predictions are outside of the measurement errors. The highest observed TEC during the 2015 event is on 26 March 2015, which is likely affected by the M3.0 solar flare that occurred almost two days before the RO measurement.

These empirical models are based on various observations at solar wind steady conditions or averaged conditions and do not take any SEP information into consideration. Ideally deviations from models can be used to identify how the ionosphere changes with local atmospheric conditions and how it is coupled with external factors. However, the models are based on a large set of data while here we use only a few points for comparison. There is a fairly good agreement for the 2011 event but the over prediction is noticeable for the 2015 event. For both events the profiles are on southern latitudes around $L_s = 300^\circ$ where the dust show some inter annual variability between MY30 and MY32 which may affect the scale height variation with altitude. In addition, the commonly used $F_{10.7}$ solar proxy may not be the most realistic characterization of the ionizing flux on Mars and alternatives like summing the photon flux can be considered (Girazian et al., 2011).

4. Discussion and Conclusions

The effects of two solar events in June 2011 and February–March 2015, on Mars's upper atmosphere are investigated using MaRS observations. These events were observed by various in-situ instruments onboard MEX

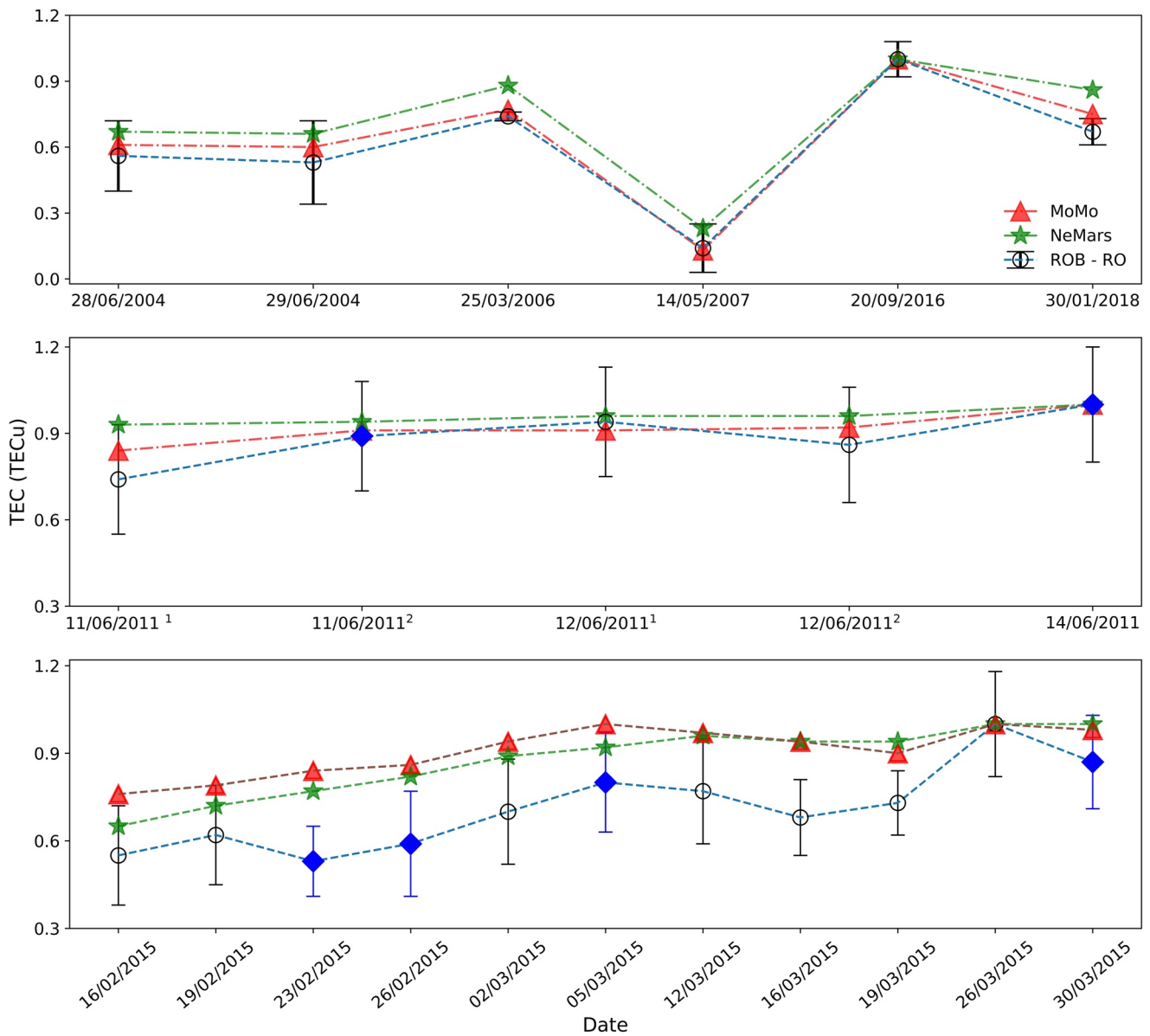


Figure 6. Comparison of normalized TEC - NeMars, MoMo, and ROB - RO (TEC obtained from RO data) for (a) four MaRS and two MAVEN data sets (from Figure 2), note that the TEC value for 14/05/2007 is very low compared to other data points as its SZA >90° (b) 2011 event and (c) 2015 event (the blue diamonds indicate that the data point is located near a crustal magnetic field). The comparison shows that the measured and modeled TEC follow a similar trend with the models mostly overestimating the TEC. 1TECu = 10¹⁶ electrons per m².

(Morgan et al., 2014) as well as MAVEN (Jakosky et al., 2015; Lee et al., 2017), and the perturbations on the Mars ionosphere were well documented. Coinciding with these events, we identified in total 16 previously unexplored residual Doppler measurements (level 2) available in the European Space Agency's Planetary Science Archive (PSA). These Doppler residuals are used to obtain the electron density profiles and TEC with the ROB RO data analysis code which is validated with published MAVEN and MEX data sets.

For both events, the effects of solar events were observable in Mars's upper atmosphere for up to several weeks where the influence decays gradually following the peak intensity at the arrival of CME. The available MaRS measurements obtained are usually several days apart from peak activity. The electron density profiles for the solar events observed in June 2011 and February–March 2015 showed no large changes in the overall electron density structure. A gradual decrease in the altitude of M2 peak density was observed for the 2011 June event, which could be due to the perturbed ionosphere going back to its original state. In the case of February–March

2015 event, the effect of solar activity is mostly seen in the topside ionosphere as an abrupt change in the scale height at around 200 km altitude within 1–4 days following a high-impact CME or flare. However, these conclusions must be considered with caution since the 11 RO observations made during the 2015 event period are close to the terminator which makes them susceptible to rapid changes.

Estimation of an absolute value of TEC by different techniques can be challenging since even the TEC obtained using the same data set may yield different results and any attempt to explain such differences has not been successful (Sánchez-Cano et al., 2015). The multi-instrument observations are also challenging due to the intrinsic limitations of each technique. The electron density profiles on Mars by RO are usually determined above 100 km of the surface, and radar data provide the profiles above the M1 peak (Morgan et al., 2008) whereas the range of in-situ measurement by Langmuir Probe and Waves (LPW) on board MAVEN (Andrews et al., 2015) is limited by the minimum altitudes of the spacecraft. The preliminary investigation of multi-instrument observations will be pursued as the follow-up to the present study (Karatekin et al., 2022). Here, rather than the absolute value of TEC, its trend provides more insights into understanding the ionosphere. In the present study, the trend of the measured TEC variations was overall in good agreement with the predictions, considering the uncertainty bounds, with no indications of variations due to solar events.

The data set used in the present study underlines the significance of the availability of RO data close to the time and location of the arrival of solar particles. The RO data we currently have does not coincide exactly with the arrival of solar particles on Mars. In June 2011, all the RO measurements are obtained five days after the peak perturbation is observed. Similarly, in the case of the February–March 2015 event, the RO measurements are mostly made 1–4 days earlier or later than the peak events. This, in fact, points to the necessity of having continuous monitoring of the ionosphere and solar activities impacting Mars's atmosphere, if possible simultaneously, by both in-situ as well as remote sensing techniques.

Data Availability Statement

The Mars Atmosphere Volatile Evolution—Radio Occultation Science Experiment data used in this paper is available at <https://lasp.colorado.edu/maven/sdc/public/pages/datasets/rose.html> and, Mars EXpress—Mars express orbiter Radio Science data are from <https://archives.esac.esa.int/psa/#!/Table%20View/MaRS=instrument>. The output files of the radio occultation data analysis software used in this study are available online at <https://doi.org/10.17605/OSF.IO/MXHCG> (Krishnan (2023)). The radio occultation data analysis software used in this paper is developed at the Royal Observatory of Belgium and is available on request at <https://forms.gle/z3Gg4S4fzy9HzkzX6>.

Acknowledgments

The authors are thankful to Bart Van Hove, Ahmed El Fadhel, and Julien Devron for their support in developing the radio occultation analysis software at different stages of its development. We are grateful to Nicolas Bergeot for providing his numerical model for the study. We also thank David P. Hinson and Paul Withers for all the valuable discussions we had. Ananya Krishnan is grateful for the grant support from Archival Research Visitor Programme, European Space Agency. Ozgur Karatekin acknowledges the Belgian Science Policy Office (BELSPO), with the financial and contractual coordination by the ESA Prodx Office (PEA 4000103401, 4000121493). B.S.-C. acknowledges support through STFC Ernest Rutherford Fellowship ST/V004115/1.

References

- Andrews, D. J., Andersson, L., Delory, G. T., Ergun, R. E., Eriksson, A. I., Fowler, C. M., et al. (2015). Ionospheric plasma density variations observed at Mars by MAVEN/LPW. *Geophysical Research Letters*, 42(21), 8862–8869. <https://doi.org/10.1002/2015GL065241>
- Barabash, S., Lundin, R., Andersson, H., Brinkfeldt, K., Grigoriev, A., Gunell, H., et al. (2006). The analyzer of space plasmas and energetic atoms (ASPERA-3) for the Mars express mission. *Space Science Reviews*, 126(1–4), 113–164. <https://doi.org/10.1007/s11214-006-9124-8>
- Bergeot, N., Witasse, O., Le Maistre, S., Blelly, P. L., Kofman, W., Peter, K., et al. (2019). Momo: A new empirical model of the Mars ionospheric total electron content based on Mars express marsis data. *Journal of Space Weather and Space Climate*, 9(A36), A36. <https://doi.org/10.1051/swsc/2019035>
- Connerney, J. E. P., Acuña, M. H., Ness, N. F., Kletetschka, G., Mitchell, D. L., Lin, R. P., & Reme, H. (2005). Tectonic implications of Mars crustal magnetism. *Proceedings of the National Academy of Sciences of the United States of America*, 102(42), 14970–14975. <https://doi.org/10.1073/pnas.050746910>
- Dubinin, E., Fraenz, M., Andrews, D., & Morgan, D. (2016). Martian ionosphere observed by Mars express. 1. Influence of the crustal magnetic fields. *Planetary and Space Science*, 124, 62–75. <https://doi.org/10.1016/j.pss.2016.02.004>
- Eparvier, F., Chamberlin, P., Woods, T., & Thiemann, E. (2015). The solar extreme ultraviolet monitor for maven. *Space Science Reviews*, 195(1–4), 293–301. <https://doi.org/10.1007/s11214-015-0195-2>
- Eshleman, V. R. (1973). The radio occultation method for the study of planetary atmospheres. *Planetary and Space Science*, 21(9), 1521–1531. [https://doi.org/10.1016/0032-0633\(73\)90059-7](https://doi.org/10.1016/0032-0633(73)90059-7)
- Felici, M., Withers, P., Smith, M. D., González-Galindo, F., Oudrhiri, K., & Kahan, D. (2020). MAVEN ROSE observations of the response of the Martian ionosphere to dust storms. *Journal of Geophysical Research: Space Physics*, 125(6), e2019JA027083. <https://doi.org/10.1029/2019JA027083>
- Fjeldbo, G., Kliore, A., & Seidel, B. (1970). The mariner 1969 occultation measurements of the upper atmosphere of Mars. *Radio Science*, 5(2), 381–386. <https://doi.org/10.1029/RS005i002p00381>
- Fjeldbo, G., Kliore, A. J., & Eshleman, V. R. (1971). The neutral atmosphere of Venus as studied with the mariner v radio occultation experiments. *The Astronomical Journal*, 76, 123. <https://doi.org/10.1086/111096>
- Fox, J. L., Galand, M. I., & Johnson, R. E. (2008). Energy deposition in planetary atmospheres by charged particles and solar photons. *Space Science Reviews*, 139(1–4), 3–62. <https://doi.org/10.1007/s11214-008-9403-7>

- Girazian, Z. R., Withers, P., Fallows, K., Paetzold, M., & Tellmann, S. (2011). How Chapman-like is the ionosphere of Mars? In *Agu Fall Meeting Abstracts* (Vol. 2011, pp. SA13A–1879).
- Gurnett, D. A., Huff, R. L., Morgan, D. D., Persoon, A. M., Averkamp, T. F., Kirchner, D. L., et al. (2008). An overview of radar soundings of the Martian ionosphere from the Mars express spacecraft. *Advances in Space Research*, *41*(9), 1335–1346. <https://doi.org/10.1016/j.asr.2007.01.062>
- Gurnett, D. A., Kirchner, D. L., Huff, R. L., Morgan, D. D., Persoon, A. M., Averkamp, T. F., et al. (2005). Radar soundings of the ionosphere of Mars. *Science*, *310*(5756), 1929–1933. <https://doi.org/10.1126/science.1121868>
- Haider, S. (2012). Role of solar x-ray flares and CME in the E region ionosphere of Mars: MGS observations. *Planetary and Space Science*, *63–64*, 56–61. <https://doi.org/10.1016/j.pss.2011.11.007>
- Haider, S. A., Abdu, M. A., Batista, I. S., Sobral, J. H., Kallio, E., Maguire, W. C., & Verigin, M. I. (2009). On the responses to solar x-ray flare and coronal mass ejection in the ionospheres of Mars and Earth. *Geophysical Research Letters*, *36*(13), 9805–9825. <https://doi.org/10.1029/2009GL038694>
- Hurley, K., Mitrofanov, I., Kozyrev, A., Litvak, M., Grinkov, A., Charyshnikov, S., et al. (2008). Mars odyssey joins the third interplanetary network. *The Astrophysical Journal - Supplement Series*, *164*(1), 124–129. <https://doi.org/10.1086/501352>
- Jakosky, B. M., Grebowsky, J. M., Luhmann, J. G., Connerney, J., Eparvier, F., Ergun, R., et al. (2015). MAVEN observations of the response of Mars to an interplanetary coronal mass ejection. *Science*, *350*(6261). <https://doi.org/10.1126/science.aad0210>
- Jakowski, N. (2005). Radio occultation techniques for probing the ionosphere. *URSI Radio Science Bulletin*, *2005*(314), 4–15. <https://doi.org/10.23919/URSIRSB.2005.7909740>
- Karatekin, Ö., Krishnan, A., Verkercke, S., Henry, G., Sánchez-Cano, B., & Witasse, O. (2022). Multi-instrument/spacecraft observations of Mars upper atmosphere electron density. In *Europlanet Science Congress 2022* (p. EPSC2022). Granada, Spain, 18–23 Sep 2022. <https://doi.org/10.5194/eps2022-688>
- Kawabata, Y., Iida, Y., Doi, T., Akiyama, S., Yashiro, S., & Shimizu, T. (2018). Statistical relation between solar flares and coronal mass ejections with respect to sigmoidal structures in active regions. *The Astrophysical Journal*, *869*(2), 99. <https://doi.org/10.3847/1538-4357/aabfcf>
- Kerstin, P., Pätzold, M., Molina-Cuberos, G. J., González-Galindo, F., Witasse, O., Tellmann, S., et al. (2021). The lower dayside ionosphere of Mars from 14 years of Mars radio science observations. *Icarus*, *359*, 114213. <https://doi.org/10.1016/j.icarus.2020.114213>
- Klein, K.-L., & Dalla, S. (2017). Acceleration and propagation of solar energetic particles. *Space Science Reviews*, *212*(3–4), 1107–1136. <https://doi.org/10.1007/s11214-017-0382-4>
- Kliore, A., Cain, D. L., Levy Gerald, S., Eshleman, V. R., Fjeldbo, G., & Drake, F. D. (1965). Occultation experiment: Results of the first direct measurement of Mars's atmosphere and ionosphere. *Science*, *149*(3689), 1243–1248. <https://doi.org/10.1126/science.149.3689.1243>
- Krishnan, A. (2023). Radio science 2011 and 2015 solar event RO analysis [collection]. <https://doi.org/10.17605/OSF.IO/MXHC8>
- Lee, C. O., Hara, T., Halekas, J. S., Thiemann, E., Chamberlin, P., Eparvier, F., et al. (2017). MAVEN observations of the solar cycle 24 space weather conditions at Mars. *Journal of Geophysical Research: Space Physics*, *122*(3), 2768–2794. <https://doi.org/10.1002/2016JA023495>
- Lillis, R. J., Frey, H. V., & Manga, M. (2008). Rapid decrease in Martian crustal magnetization in the Noachian era: Implications for the dynamo and climate of early Mars. *Geophysical Research Letters*, *35*(14), L14203. <https://doi.org/10.1029/2008GL034338>
- Mendillo, M., Withers, P., Hinson, D., Rishbeth, H., & Reinisch, B. (2006). Effects of solar flares on the ionosphere of Mars. *Science*, *311*(5764), 1135–1138. <https://doi.org/10.1126/science.1122099>
- Morgan, D. D., Diéval, C., Gurnett, D. A., Duru, F., Dubinin, E. M., Fränz, M., et al. (2014). Effects of a strong ICME on the Martian ionosphere as detected by Mars express and Mars odyssey. *Journal of Geophysical Research: Space Physics*, *119*(7), 5891–5908. <https://doi.org/10.1002/2013JA019522>
- Morgan, D. D., Gurnett, D. A., Kirchner, D. L., Fox, J. L., Nielsen, E., & Plaut, J. J. (2008). Variation of the Martian ionospheric electron density from Mars express radar soundings. *Journal of Geophysical Research*, *113*(A9), A09303. <https://doi.org/10.1029/2008JA013313>
- Nagy, A. F., & Banks, P. M. (1970). Photoelectron fluxes in the ionosphere. *Journal of Geophysical Research*, *75*(31), 6260–6270. <https://doi.org/10.1029/JA075i031p06260>
- Pätzold, M., Häusler, B., Tyler, G. L., Andert, T., Asmar, S. W., Bird, M. K., et al. (2016). Mars express 10 years at Mars: Observations by the Mars express radio science experiment (Mars). *Planetary and Space Science*, *127*, 44–90. <https://doi.org/10.1016/j.pss.2016.02.013>
- Pätzold, M., Neubauer, F. M., Carone, L., Hagermann, A., Stanzel, C., Häusler, B., et al. (2004). *Mars: Mars express orbiter radio science* (Vol. 1240).
- Riedler, W., Möhlmann, D., Oraevsky, V. N., Schwingenschuh, K., Yeroshenko, Y., Rustenbach, J., et al. (1989). Magnetic fields near Mars: First results. *Nature*, *341*(6243), 604–607. <https://doi.org/10.1038/341604a0>
- Sánchez-Cano, B., Lester, M., Witasse, O., Milan, S. E., Hall, B. E. S., Cartacci, M., et al. (2016). Solar cycle variations in the ionosphere of Mars as seen by multiple Mars express data sets. *Journal of Geophysical Research: Space Physics*, *121*(3), 2547–2568. <https://doi.org/10.1002/2015JA022281>
- Sánchez-Cano, B., Morgan, D. D., Witasse, O., Radicella, S. M., Herraiz, M., Orosei, R., et al. (2015). Total electron content in the Martian atmosphere: A critical assessment of the Mars express marsis data sets. *Journal of Geophysical Research: Space Physics*, *120*(3), 2166–2182. <https://doi.org/10.1002/2014JA020630>
- Sánchez-Cano, B., Radicella, S. M., Herraiz, M., Witasse, O., & Rodríguez-Caderot, G. (2013). Nemars: An empirical model of the Martian dayside ionosphere based on Mars express marsis data. *Icarus*, *225*(1), 236–247. <https://doi.org/10.1016/j.icarus.2013.03.021>
- Thampi, S. V., Krishnaprasad, C., Nampoothiri, G. G., & Pant, T. K. (2021). The impact of a stealth CME on the Martian topside ionosphere. *Monthly Notices of the Royal Astronomical Society*, *503*(1), 625–632. <https://doi.org/10.1093/mnras/stab494>
- Tsurutani, B. T., Verkhoglyadova, O. P., Mannucci, A. J., Lakhina, G. S., Li, G., & Zank, G. P. (2009). A brief review of “solar flare effects” on the ionosphere. *Radio Science*, *44*(1). <https://doi.org/10.1029/2008RS004029>
- Ulusen, D., Brain, D. A., Luhmann, J. G., & Mitchell, D. L. (2012). Investigation of Mars' ionospheric response to solar energetic particle events. *Journal of Geophysical Research*, *117*(A12), A12306. <https://doi.org/10.1029/2012JA017671>
- Wang, J., Yue, X., Wei, Y., & Wan, W. (2018). Optimization of the Mars ionospheric radio occultation retrieval. *Earth and Planetary Physics*, *2*(4), 1–11. <https://doi.org/10.26464/epp2018027>
- Witasse, O., Cravens, T., Mendillo, M., Moses, J., Kliore, A., Nagy, A. F., & Breus, T. (2008). Solar system ionospheres. *Space Science Reviews*, *139*(1–4), 235–265. <https://doi.org/10.1007/s11214-008-9395-3>
- Withers, P., Fallows, K., Girazian, Z., Matta, M., Häusler, B., Hinson, D., et al. (2012). A clear view of the multifaceted dayside ionosphere of Mars. *Geophysical Research Letters*, *39*(18), L18202. <https://doi.org/10.1029/2012GL053193>
- Withers, P., Felici, M., Hensley, K., Mendillo, M., Barbinis, E., Kahan, D., et al. (2023). The ionosphere of Mars from solar minimum to solar maximum: Dayside electron densities from MAVEN and Mars global surveyor radio occultations. *Icarus*, *393*, 114508. <https://doi.org/10.1016/j.icarus.2021.114508>

- Withers, P., Felici, M., Mendillo, M., Moore, L., Narvaez, C., Vogt, M. F., et al. (2020). The MAVEN radio occultation science experiment (ROSE). *Space Science Reviews*, 216(61), 1–49. <https://doi.org/10.1007/s11214-020-00687-6>
- Withers, P., Felici, M., Mendillo, M., Vogt, M. F., Barbinis, E., Kahan, D., et al. (2022). Observations of high densities at low altitudes in the nightside ionosphere of Mars by the maven radio occultation science experiment (ROSE). *Journal of Geophysical Research: Space Physics*, 127(11), e2022JA030737. <https://doi.org/10.1029/2022JA030737>
- Withers, P., & Moore, L. (2020). How to process radio occultation data: 2. From time series of two-way, single-frequency frequency residuals to vertical profiles of ionospheric properties. *Radio Science*, 55(8). <https://doi.org/10.1029/2019RS007046>
- Withers, P., Moore, L., Cahoy, K., & Beerer, I. (2014). How to process radio occultation data: 1. From time series of frequency residuals to vertical profiles of atmospheric and ionospheric properties. *Planetary and Space Science*, 101, 77–88. <https://doi.org/10.1016/j.pss.2014.06.011>
- Zhang, S. J., Cui, J., Guo, P., Li, J. L., Ping, J. S., Jian, N. C., & Zhang, K. F. (2015). Martian electron density profiles retrieved from Mars express dual-frequency radio occultation measurements. *Advances in Space Research*, 55(9), 2177–2189. <https://doi.org/10.1016/j.asr.2015.01.030>